Int. J. Multiphase Flow Vol. 16, No. 2, pp. 281–294, 1990
Printed in Great Britain.

0301-9322/90 $3.00 + 0.00

ANNULAR FLOW AT HIGH EVAPORATION RATES

J. NAHSTOLL†
German Aerospace Research Establishment (DFVLR), 7101 Lampoldshausen, F.R.G.

(*Received* 1 *October* 1988; *in revised form* 8 *August* 1989)

Abstract—The process of liquid film cooling of combustion chamber walls which are subjected to extremely high heat rates was investigated. A theoretical model has been developed for a reliable prediction of the film cooling length. The mass transfer at the liquid–gas interface results from evaporated liquid and entrained liquid droplets. The film cooling length analysis, which includes the physical effects in detail, is separated into two regions: heating the liquid and evaporating the liquid. The theoretical results were experimentally verified at high pressures and temperatures using a modified H_2/O_2 rocket motor. There is a good agreement between the theoretical and the experimental results over the experimental range.

Key Words: H_2/O_2 combustion chamber, liquid film cooling, film cooling length, annular two-phase-flow, interaction liquid film–gas flow

INTRODUCTION

Liquid film cooling provides an attractive means of protecting the inner surfaces of combustion chamber walls which are subjected to extremely high heat rates. A thin continuous liquid layer is injected between the wall surface and the hot gas stream and forms an annular flow (figure 1).

The most important parameter for liquid film cooling design is the film cooling length, L. This corresponds to the length after which the liquid film is evaporated and must be replaced by establishing a new film. The length L is dependent on the following mass flow rates: entrained droplets at the injection point, evaporated and entrained droplets from the film surface, deposited droplets on the liquid film.

The aim of the investigation described below was to develop a theoretical model for a reliable prediction of the film cooling length. This model includes more of the physical effects at the shear driven liquid film such as film stability or film roughness than previous models. The theoretical results have been verified at high pressures and temperatures with the aid of a modified rocket motor and previous experimental data.

EXPERIMENTAL INSTALLATION

All of the experiments reported herein were conducted within the 100 mm dia, cylindrical combustion chamber of a modified rocket motor burning the gaseous propellants hydrogen and oxygen in a stoichiometric mixture ratio. The reaction product temperature of approx. 3500 K could be reduced arbitrarily by central injection of water. Pressure and velocity of the gas stream were also varied over a wide range by changing the propellant flow rate and the throat area of the exhaust nozzle. Mixture ratio, pressure and temperature were held constant by a digital control system (Wolfmüller 1984). Figure 2 presents a longitudinal cross-sectional view through the experimental motor. The film coolant water was introduced to the inner surface through 300 circumferentially arranged holes of 0.5 mm dia. The uniformly spaced holes had an inclination of 15° relative to the gas velocity to make sure that there was no penetration of the film coolant at the point of injection (Nahstoll 1988). The total film coolant mass flow rate was varied between 15 and 200 g/s and was held constant with the help of a pneumatically operated regulator.

The film cooling length was determined by measuring the temperature rise of the inner surface of the film cooled test section mounted downstream of the injection point. The wall temperature thermocouples were mounted in a 10 mm axial distance and 0.5 mm inset in the wall surface. This

†Present address: BASF AG, ZET/ZD-A15, 6700 Ludwigshafen, F.R.G.

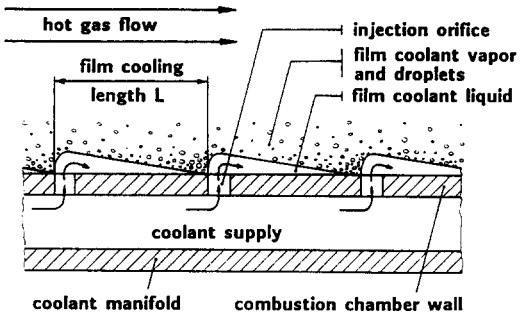

Figure 1. Film cooled combustion chamber.

test section was not cooled externally; its protection from the hot gases being effected entirely by the liquid film.

THEORETICAL MODEL FOR PREDICTING THE FILM COOLING LENGTH

A theoretical modelling of the flow and transport phenomena was possible under the following assumptions:

(1) steady state and cylindrical symmetrical two-phase flow;
(2) constant gas properties over the film cooling length;
(3) unstable liquid film (droplet entrainment and deposition);
(4) mean film thickness negligible with respect to the duct diameter;
(5) mean film velocity negligible with respect to mean gas velocity;
(6) interfacial shear stress is the dominating force for describing the liquid film–gas interaction;
(7) roughness height of the wavy liquid surface can be described with the help of the equivalent sandgrain roughness;
(8) heat transfer between the hot gas and the liquid film is due to a convective and a radiative term.

The heat and mass transfer rates at the liquid film must be known for the calculation of the film cooling length. The complexity of the interfacial phenomena made a pure theoretical description dependent on the working length, z, impossible (Nahstoll 1988). So empirical laws were used, describing the phenomena at a finite film section.

The film cooling length analysis is separated into two finite regions according to figure 3. In each of the two regions, the values of the influencing parameters are averaged over the region. For the very thin liquid films (characteristic thickness $d_L \approx 0.1$ mm), the thickness and the temperature T_L are assumed to be linearly dependent on the working length, z.

In region 1, the liquid heating region, the liquid is injected at the point $z = 0$ with the initial temperature T_i and heated up to saturation temperature T_s, at point $z = L_1$ with no evaporation occurring.

In region 2, the liquid evaporation region, the liquid film is evaporated until point $z = L_2$ at the constant temperature T_s.

The mass balance is averaged over the film surface A ($A = B \cdot L$) and circumference B. The terms included are: the mass flow rate of the film $\dot{m}_{B,L}$, the mass flow rate of entrained droplets $\dot{m}_{A,en}$, the mass flow rate of deposited droplets $\dot{m}_{A,de}$ and the mass flow rate of the vapor $\dot{m}_{A,v}$.

The energy balance is also averaged over the wetted surface A and the width of the liquid film B. The terms included are: the enthalpy flux of the film $\dot{H}_{B,L}$, the convective heat flux between gas and liquid $\dot{q}_{c,GL}$, the radiative heat flux between gas and liquid $\dot{q}_{r,GL}$, the convective heat flux between liquid and wall $\dot{q}_{c,LW}$ and the enthalpy flux of the vapor $\dot{q}_v$.

If the following dependencies are taken into consideration:

$$\dot{H}_{B,L,i} = \dot{m}_{B,L,i} h_i, \qquad [1]$$

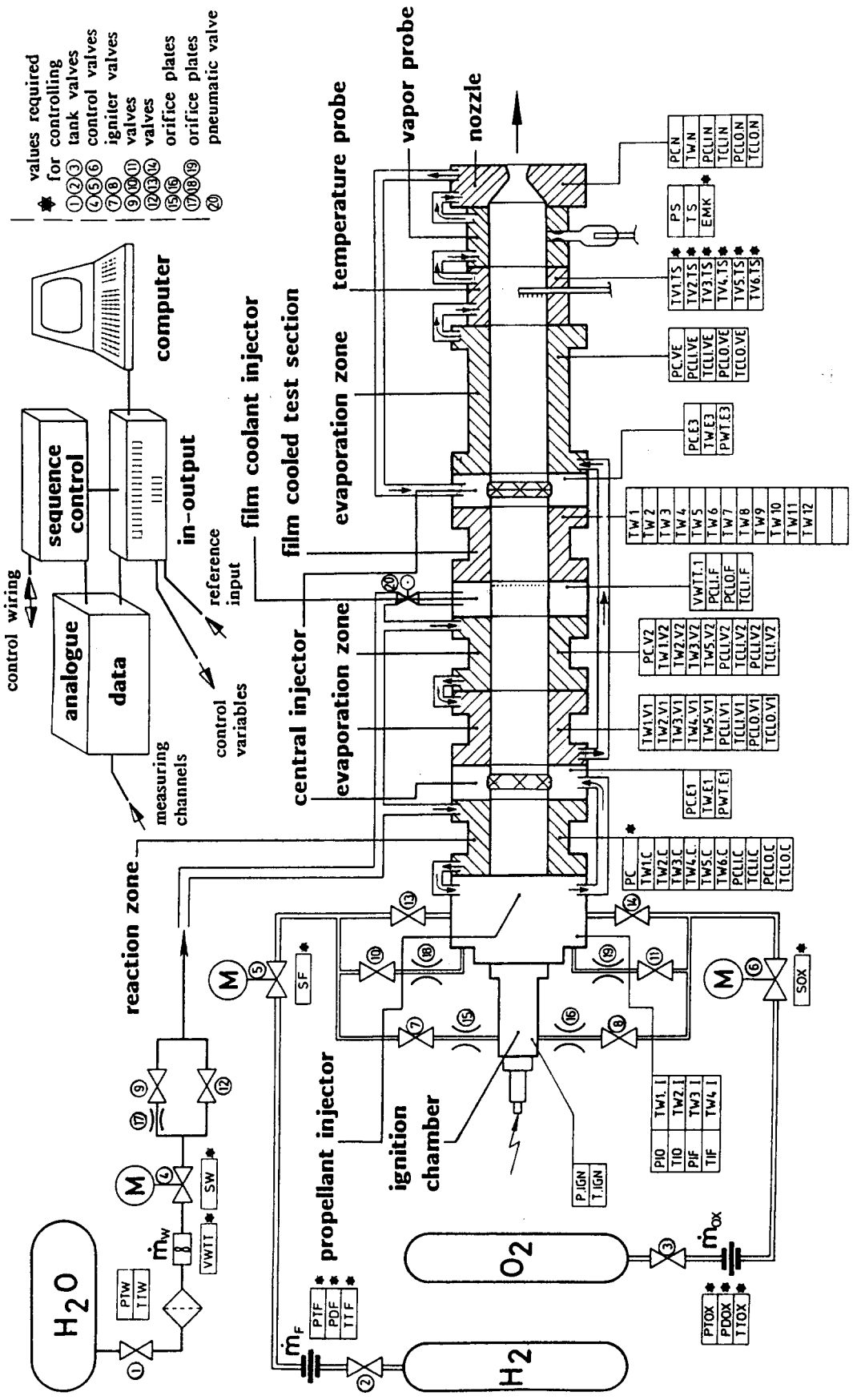

Figure 2. Experimental rocket motor and supply system.

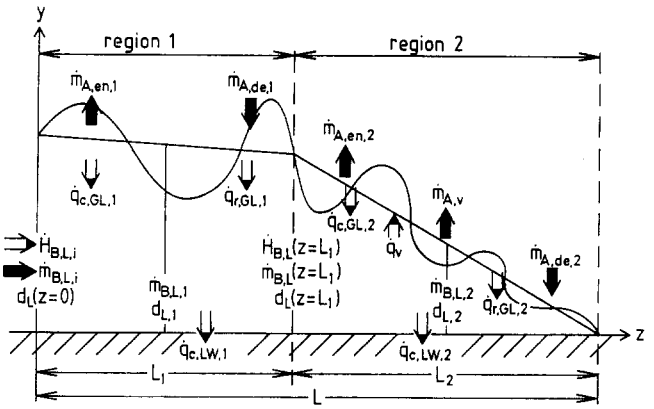

Figure 3. Heat and mass balance diagram at the liquid film.

$$\dot{q}_v = \dot{m}_{A,v} h_v, \quad [2]$$

$$\dot{H}_{B,L}(z = L_1) = \dot{m}_{B,L}(z = L_1) h_s \quad [3]$$

and

$$\Delta h_v = h_v - h_s; \quad [4]$$

the mass and energy balances for the regions 1 and 2 according to figure 3 result in the following equations for the lengths L_1 and L_2:

$$L_1 = \frac{\dot{m}_{B,L,i}(h_s - h_i)}{\dot{q}_{c,GL,1} + \dot{q}_{r,GL,1} - \dot{q}_{c,LW,1} + (\dot{m}_{A,en,1} - \dot{m}_{A,de,1}) h_s} \quad [5]$$

and

$$L_2 = \frac{\dot{m}_{B,L}(z = L_1)\,\Delta h_v}{\dot{q}_{c,GL,2} + \dot{q}_{r,GL,2} - \dot{q}_{c,LW,2} + (\dot{m}_{A,en,2} - \dot{m}_{A,de,2}) h_v}; \quad [6]$$

h is enthalpy and Δh_v is the heat of vaporization. The subscripts stand for the following conditions: "A" means per unit area of liquid film, "B" per unit width of liquid film; "L" means liquid film, "i" describes the conditions at the injection point, "v" the saturated vapor and "s" the boiling conditions; "1" means averaged over region 1, "2" over region 2, respectively.

Starting out from the above-mentioned assumptions, figure 4 shows the process of liquid film cooling at an arbitrary place inside the combustion chamber. The distance $z' = Z_E$ between propellant injector and film coolant injector is defined as the entrance region.

THEORETICAL BACKGROUND

The heat fluxes are estimated with the assumption that the liquid film could be described as a very thin, rough and wavy layer which adheres to the wall surface.

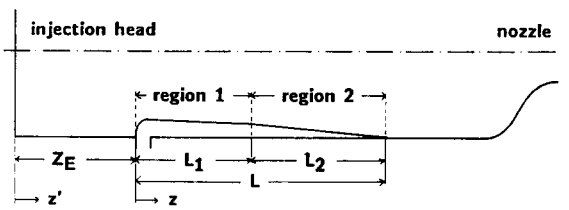

Figure 4. Simplified description of the film cooling process in the combustion chamber.

The convective heat flux is calculated from

$$\dot{q}_{c,GL} = \frac{\lambda_G Nu_G}{D}(T_G - T_L)K_t K_r K_b K_c = \dot{q}_{c,GL,id} K_t K_r K_b K_c \quad [7]$$

based on a Nusselt number equation of Gnielinski (1975),

$$Nu_G = 0.0214(Re_G^{0.8} - 100)Pr_G^{0.4}\left[1 + \left(\frac{D}{Z}\right)^{2/3}\right], \quad [8]$$

using the entrance conditions of a circular tube for turbulent flow. Nu is the Nusselt number, λ is the thermal conductivity, T is the temperature, Re is the Reynolds number, Pr is the Prandtl number, D is the diameter and Z is the length of the cylindrical combustion chamber. The subscript "G" describes the conditions of the superheated gas flow.

The correction factors K_t, K_r, K_b and K_c, which account for the special effects at the film surface are discussed subsequently. Neglecting these factors leads to the "ideal" convective heat flux $\dot{q}_{c,GL,id}$. The calculations provided ideal convective heat fluxes between 1.8 and 2.5 times lower than the heat fluxes considering the correction factors. K_t describes the influence of temperature-dependent fluid properties at the very high temperature differences between the wall surface (=liquid film) and the gas stream. It is calculated by a correlation of Gregorig (1970), considering the influences of thermal conductivity λ, kinematic viscosity ν, Prandtl number Pr and dimensionless tube length Z/D:

$$K_t = \frac{K_\lambda K_{Pr}}{K_\nu}, \quad [9]$$

$$K_\lambda = \left(\frac{\lambda_v}{\lambda_G}\right)^{2\{1-\exp[-0.185(Z/D)^{1/3}]\}[(\lambda_{ref}-\lambda_v)/(\lambda_G-\lambda_v)]}, \quad [10]$$

$$K_{Pr} = \left(\frac{Pr_v}{Pr_G}\right)^{1.44\{1-\exp[-0.185(Z/D)^{1/3}]\}[(Pr_{ref}-Pr_v)/(Pr_G-Pr_v)]} \quad [11]$$

and

$$K_\nu = \left(\frac{\nu_v}{\nu_G}\right)^{1.88\{1-\exp[-0.185(Z/D)^{1/3}]\}[(\nu_{ref}-\nu_v)/(\nu_G-\nu_v)]}. \quad [12]$$

The reference temperature for estimating λ_{ref}, Pr_{ref} and ν_{ref} is defined as

$$T_{ref} = 0.5(T_G + T_L). \quad [13]$$

K_r is the correction factor for the rough liquid surface. It is calculated by an empirical correlation of Burck (1969). He defined an efficiency μ for integral roughness and fully roughened surfaces,

$$\mu = \frac{\frac{Nu_{ro}}{Nu_{sm}}}{\frac{\zeta_{ro}}{\zeta_{sm}}} = \frac{K_r}{\frac{\zeta_{ro}}{\zeta_{sm}}}, \quad [14]$$

describing the increase of heat transfer at a rough channel in comparison to a smooth one; ζ is the friction factor, the subscripts "sm" and "ro" stand for the smooth and the rough channel surface, respectively. Burck found the following expression for the efficiency:

$$\mu = \log_{10}\left[\frac{Pr_G^{0.33}}{k_s^{+0.243}}\right] - 0.32 \cdot 10^{-3} k_s^+ \cdot \log_{10} Pr_G + 1.25, \quad [15]$$

where k_s^+ is the dimensionless roughness height.

For shear driven liquid films the roughness height k_s of the film is estimated as twice the mean film thickness d_L (Shearer & Neederman 1965; Wurz 1979),

$$k_s = 2d_L. \quad [16]$$

The mean film thickness is calculated from the interfacial shear stress τ_{in},

$$\tau_{in} = \frac{\frac{D}{2} - d_L}{2}\left(\frac{\Delta p}{Z}\right). \quad [17]$$

A number of shear stress correlations are available in the literature. Chawla (1968) formulated the following one for the pressure drop per tube length $\Delta p/z$:

$$\frac{\Delta p}{z} = \frac{0.3164}{2D\rho_G} \cdot \left[\frac{4(\dot{m}_L + \dot{m}_G)}{\pi D \eta_G}\right]^{-1/4} \left[\frac{\dot{m}_L + \dot{m}_G}{\frac{\pi D^2}{4}}\right]^2 x^{7/4} \cdot \left[1 + \frac{1-x}{x\gamma}\frac{\rho_L}{\rho_G}\right]^{19/8}, \quad [18]$$

with

$$x = \frac{\dot{m}_G}{\dot{m}_L + \dot{m}_G} \quad [19]$$

and

$$\gamma = 9.1 \frac{1-x}{x}\left[\frac{\rho_G}{\rho_L}\right]^{0.9}\left[\frac{\eta_G}{\eta_L}\right]^{0.5}\left[\frac{\eta_L g \rho_L^2}{(1-x)^3}\left(\frac{\frac{\pi D^2}{4}}{\dot{m}_L + \dot{m}_G}\right)^3\right]^{1/6}, \quad [20]$$

where ρ is the density, η is the dynamic viscosity and g is the acceleration due to gravity.

Wurz (1979) estimated the mean film thickness d_L with the help of the mass conservation law, deducing a velocity profile for the shear driven liquid film:

$$d_L = \frac{1}{2}\left[\frac{3\dot{m}_{B,L}}{\eta_L}\right]^{2/3} \frac{\eta_L}{\rho_L u_L^*}, \quad [21]$$

where u_L^* is the liquid friction velocity.

The interfacial shear stress and film thickness correlations are only valid for adiabatic flow. No correlations are available for large temperature differences between the gas stream and wall surface (= liquid surface). Nevertheless, the adiabatic flow correlations can be used as a first approximation for describing the wall cooling effect (Nahstoll 1988).

K_b, the blowing surface correction factor due to the evaporating liquid, is calculated with the help of Kays' (1972) correlation:

$$K_b = \left[\frac{\ln(1+B_h)}{B_h}\right]^{1.25}(1+B_h)^{0.25} \quad [22]$$

using the blowing parameter B_h,

$$B_h = \frac{c_{p,G}(T_G - T_s)}{\Delta h_v + c_{p,L}(T_s - T_i)}; \quad [23]$$

c_p is the specific heat capacity at constant pressure. The blowing surface leads to an increase of the boundary layer thickness compared to the non-blowing surface and therefore to a decrease of the heat flux to the wall.

K_c is the correction factor for the dependence of the physical properties of the gas on the concentration of the vapor, if gas and liquid do not have the same chemical composition. K_c is calculated by a correlation of Gater & L'Ecuyer (1969), using the results of Kays (1966):

$$K_c = \left[\frac{M_{in}}{M_G}\right]^{0.4} \quad [24]$$

with

$$\frac{1}{M_{in}} = \frac{C_{in}}{M_L} + \frac{1 - C_{in}}{M_G} \quad [25]$$

and

$$C_{in} = \frac{B_h}{1 - B_h}; \qquad [26]$$

here M is the molecular weight and C is the concentration, the subscript "in" describes the conditions at the gas–liquid interface.

The radiative heat flux $\dot{q}_{r,GL}$ is treated as water vapor radiation. It can be estimated by the following equation (VDI-Wärmeatlas 1984):

$$\dot{q}_{c,GL} = \sigma \cdot \frac{\epsilon_W}{1 - (1 - \epsilon_W)(1 - A_v)} (\epsilon_G T_G^4 - A_v T_W^4), \qquad [27]$$

here σ is the Stefan–Boltzmann radiation constant. The emission factor of the wall, ϵ_W, is dependent on the wall material (=liquid film). The emission factor of the gas, ϵ_G, is a function of partial pressure, temperature and surface area of the gas, the absorption factor, A_v, is further dependent on the wall temperature (=liquid film temperature). These factors can be estimated by empirical correlations (Hottel & Serafim 1967). For these results, the heat flux to the wall, $\dot{q}_{c,LW}$, is neglected with respect to $\dot{q}_{c,GL}$ and $\dot{q}_{r,GL}$ because of the poor thermal conductivity of the stainless steel used as wall material.

The entrained mass flow rate into the gas, $\dot{m}_{A,en}$, and the deposited mass flow rate onto the film, $\dot{m}_{A,de}$, are calculated by an empirical model, proposed by Whalley & Hewitt (1978). $\dot{m}_{A,en}$ is estimated from figure 5; $\dot{m}_{A,de}$ can be neglected for the experimentally given boundary conditions. The Whalley & Hewitt (1978) correlation, which is valid for adiabatic flow, yields too large entrainment rates in comparison with these experimental results. This could be expected. An increase of the evaporation rate, characterized by an increase of the temperature differences between gas and liquid, leads to a film stabilization. These experimental results with wall cooling can be satisfactorily correlated by the second curve in figure 5, represented by the following expressions:

$$\frac{\dot{m}_{A,en}\sigma_{in}}{\tau_{in}\eta_L} = 5\frac{\tau_{in}d_L}{\sigma_{in}} - 0.5 \qquad \text{for } \frac{\tau_{in}d_L}{\sigma_{in}} > 0.1 \qquad [28]$$

and

$$\frac{\dot{m}_{A,en}\sigma_{in}}{\tau_{in}\eta_L} = 0 \qquad \text{for } \frac{\tau_{in}d_L}{\sigma_{in}} \leqslant 0.1; \qquad [29]$$

σ_{in} is the surface tension.

THEORETICAL RESULTS

The theoretical model allows the calculation of interfacial shear stresses, mean film thicknesses, heat fluxes, mass flow rates of entrained and deposited droplets, mass flow rates of vapor and, finally, film cooling lengths for several propellant and film coolant combinations (Nahstoll 1988).

Theoretical results are shown in figures 6–8. The interfacial shear stress is plotted against the gas velocity in figure 6. The empirical models of Chawla (1968), [18]–[20], Kriegel (1967) and Hughmark (1973) are compared with the result for the wall shear stress of the single-phase flow. The correlations of Kriegel and Hughmark are not discussed here in detail but the two-phase correlations have a maximum deviation of 20%, which lies in the expected range of variations of the experimental data (Whalley & Hewitt 1978). The single-phase wall shear stress is between 20 and 40% lower than the value for annular flow.

The mean film thickness, which is mainly influenced by the interfacial shear stress, is plotted against the static pressure of the gas in figure 7. Compared here is the empirical model of Wurz (1979), [21], with the correlations of Hughmark (1973) and Shearer & Nedderman (1965). Hughmark derived his empirical model for interfacial shear stress and mean film thickness from various experimental data. Shearer & Nedderman calculated the mean film thickness with the help of the mass conservation law, assuming a linear velocity profile for the liquid film. Figure 7 shows the very good agreement between the models of Wurz and Hughmark. The correlation of Shearer

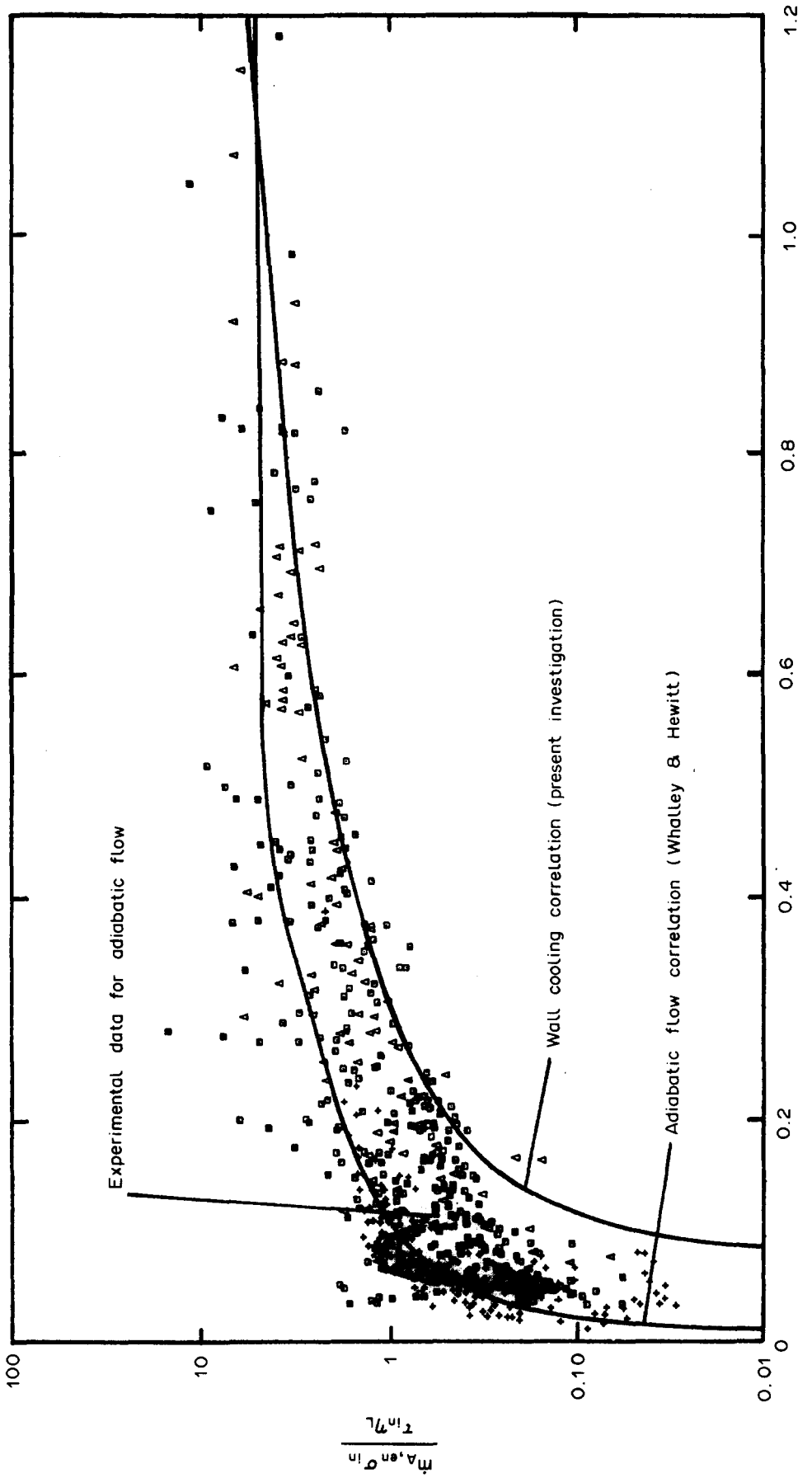

Figure 5. Entrainment rate correlation.

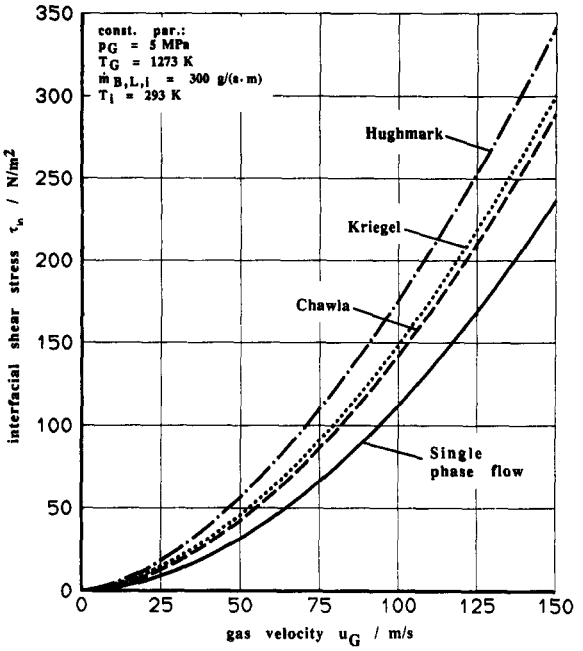

Figure 6. Variation of interfacial shear stress with gas velocity.

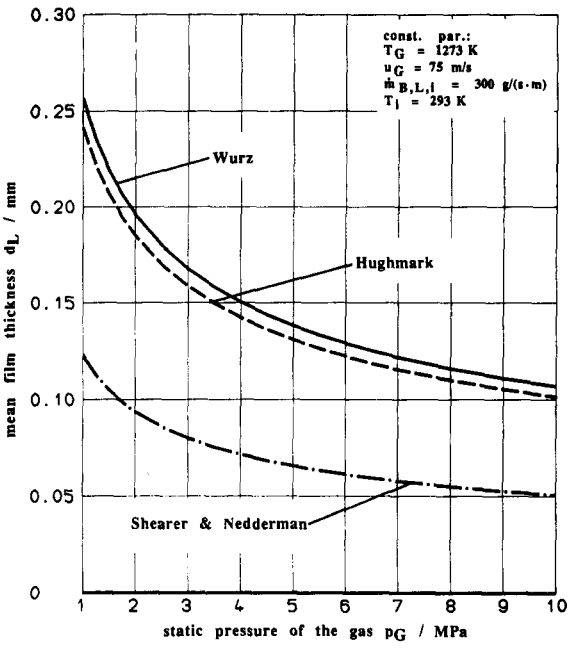

Figure 7. Variation of mean film thickness with static pressure of the gas.

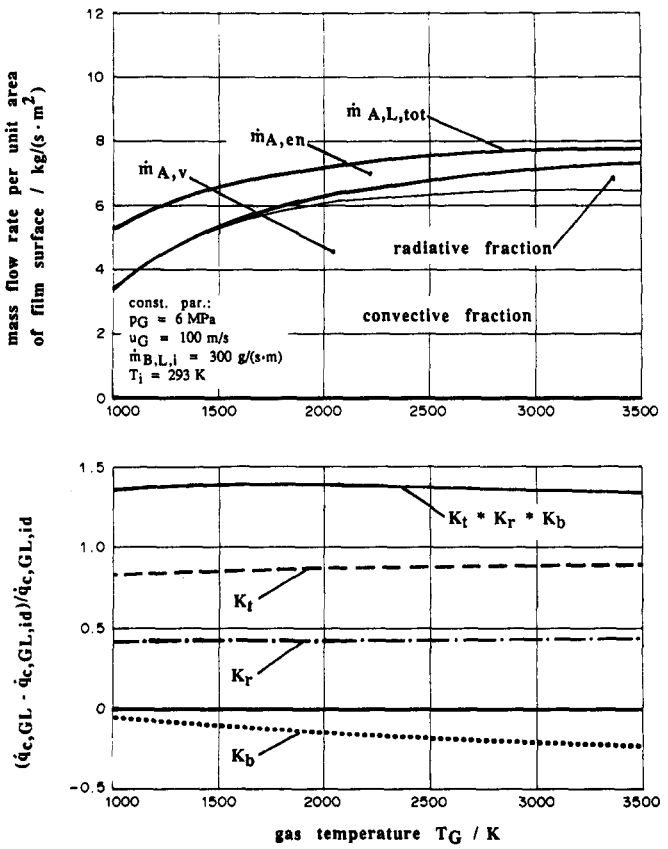

Figure 8. Variation of the mass flow rate of film coolant vapor and droplets and of the correction factors with gas temperature.

& Nedderman yields values much too low for the mean film thickness. The reason lies in assuming that the velocity profile is linear.

Figure 8 shows the liquid mass flow rate from the liquid surface to the gas flow and the relative convective heat flux to the liquid surface, dependent on the gas temperature and averaged over the film cooling length. The relative heat flux is calculated from [7], considering or neglecting the correction factors. The liquid mass flow rate per unit area of film surface $\dot{m}_{A,L,tot}$ consists of evaporated liquid $\dot{m}_{A,v}$ and entrained liquid droplets $\dot{m}_{A,en}$. The vapor mass flow rate is additionally divided into a convective and radiative fraction. The vapor mass flow rate generated by radiation is small in comparison to the one generated by convection. It reaches approx. 10% at the very high gas temperature of 3500 K. It can be seen in figure 8 that an increase in the gas temperature leads to a decrease in $\dot{m}_{A,en}$. The large increase in the radiation heat transfer with rising gas temperature is responsible for the steady increase in $\dot{m}_{A,v}$. If radiation is neglected, the vapor mass flow rate reaches a maximum and then decreases. Responsible for this phenomenon is the blowing surface correction factor K_b, which shows a large negative increase with rising gas temperature. The rough surface correction factor K_r and the temperature-dependent property correction factor K_t show only a slight positive increase with the rising gas temperature, so that the curve for the relative convective heat flux, taking all of the correction factors into account (symbol "$K_b * K_r * K_t$" in figure 8), has a maximum. This maximum is reflected in the vapor mass flow rate curve when radiative heat transfer is neglected.

EXPERIMENTAL RESULTS

The film cooling length was experimentally estimated under the following test conditions:

static pressure of the gas p_G	= 4–8 MPa
gas temperature T_G	= 1000–2800 K
gas velocity u_G	= 60–120 m/s
film coolant mass flow rate $\dot{m}_{B,L,i}$	= 50–600 g/(s m)
interfacial shear stress τ_{in}	= 40–130 N/m^2
film cooling length L	= 10–280 mm
convective heat flux $\dot{q}_{c,GL}$	= 3–13 MW/m^2
radiative heat flux $\dot{q}_{r,GL}$	= 0–3 MW/m^2.

The experimental results can be seen in figures 9(a–e). The most important parameters for describing the process of film cooling are plotted vs time. The parameters chamber pressure, gas temperature and gas velocity reach their desired values after 4 s of testing time with the help of the digital control system. The pneumatic control unit provides a constant film coolant mass flow rate after approx. 5 s. The wall temperatures measured in 10 mm axial distances starting from the injection point can be seen in figure 9(e). The wall temperature rises at a certain distance from the film coolant injector without delay after the liquid mass flow rate reaches its desired value. This significant increase in wall temperature after a certain working length of the film provided an exact estimation of the film cooling length. For the investigated interfacial shear stresses ($\tau_{in} \geqslant 40$ N/m^2), an asymmetric effect on the film cooling length generated by gravitational forces inside the horizontally mounted rocket motor could not be observed.

COMPARISON BETWEEN THEORETICAL AND EXPERIMENTAL RESULTS

Figures 10 and 11 show a comparison between the theoretical and experimental results. Experimental data are represented by bars. The film cooling length $L = L_1 + L_2$ is plotted against the film coolant mass flow rate in figure 10 and against the chamber pressure in figure 11. The theoretical results distinguish between including and neglecting the droplet entrainment effect. It can be seen in figure 10 that the liquid entrainment begins at a critical liquid mass flow rate in agreement with the experimental data. Figures 10 and 11 indicate the good agreement between the present theoretical model and the experimental results of the present investigation. Figures 12 and 13 show comparisons between experimental data and the theoretical models of Graham & Zucrow (1957), Gater & L'Ecuyer (1969) and the present investigation.

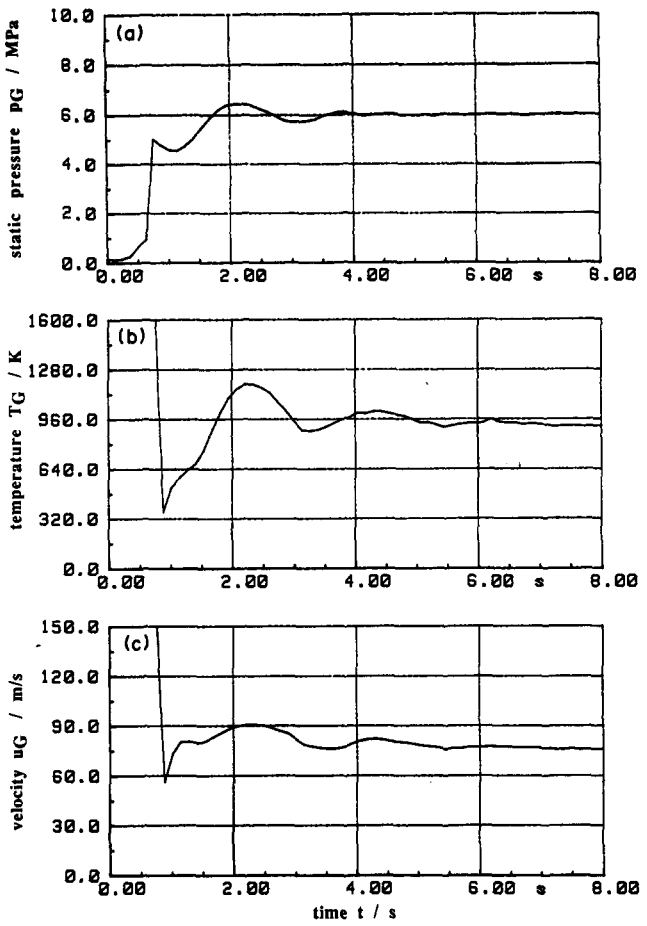

Figures 9(a–c). Variation of static pressure, temperature and velocity of the gas with time.

The main differences compared to the present theoretical model are: Graham & Zucrow (1957) formulated a semi-empirical heat transfer correlation and an empirical liquid entrainment correlation for film cooling application. They did not consider the influences of temperature-dependent fluid properties, film roughness, blowing liquid surface and dependence of the physical properties of the gas on the concentration of the vapor. Gater & L'Ecuyer used a heat transfer correlation for a flat plate. The physical effects of temperature-dependent fluid properties, film roughness and droplet entrainment were not described correctly.

Figure 12 presents a comparison between the theoretical models and the experimental data of the present investigation. There is good agreement between the present model and the experimental data. The models of Graham & Zucrow (1957) and Gater & L'Ecuyer (1969) indicate 25% too large film cooling lengths. The reason for keeping to relatively small liquid mass flow rates in Graham & Zucrow's correlation is the definition of the liquid entrainment correction factor.

In agreement with a number of already published experimental data, the models of the present investigation and of Graham & Zucrow consider a critical mass flow rate for the onset of liquid entrainment. Beyond that critical value, the theoretical curves for considering and neglecting liquid entrainment are identical. The correlation of Gater & L'Ecuyer does not consider this critical mass flow rate. There is liquid entrainment for all mass flow rates greater than zero. Additionally, the difference between the film cooling lengths for considering and neglecting the droplet entrainment effect, which is proportional to the entrained mass flow rate, is much too large and cannot be physically possible.

Figure 13 shows a comparison between the theoretical models and experimental data of Warner & Emmons (1964), represented by the circles. They conducted their experiments at much lower

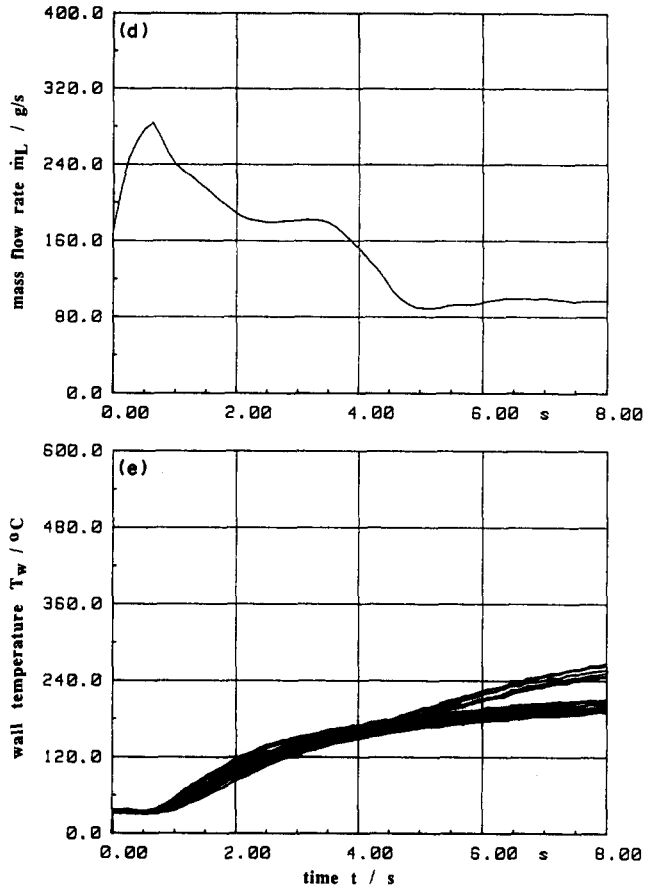

Figures 9(d, e). Variation of film coolant mass flow rate and wall temperature with time.

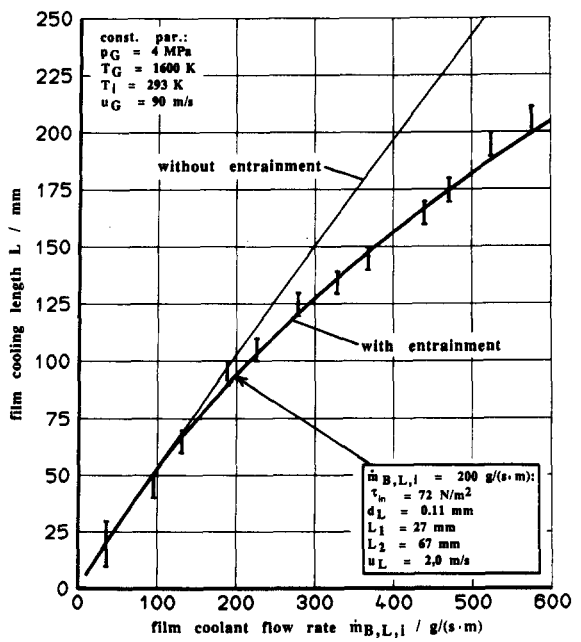

Figure 10. Comparison of present experimental and calculated values of film cooling length.

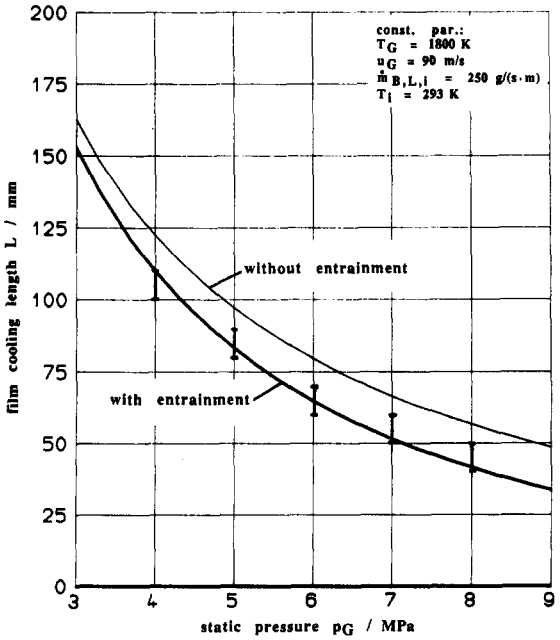

Figure 11. Comparison of present experimental and calculated values of film cooling length.

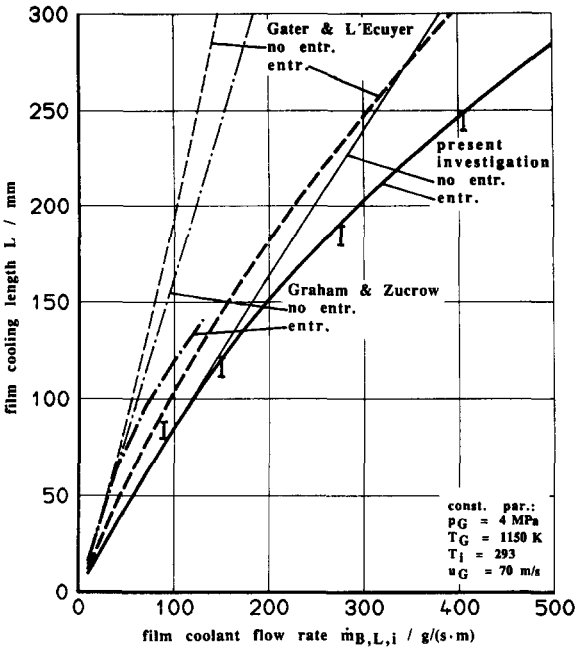

Figure 12. Comparison of present experimental data and calculated values of several theoretical models.

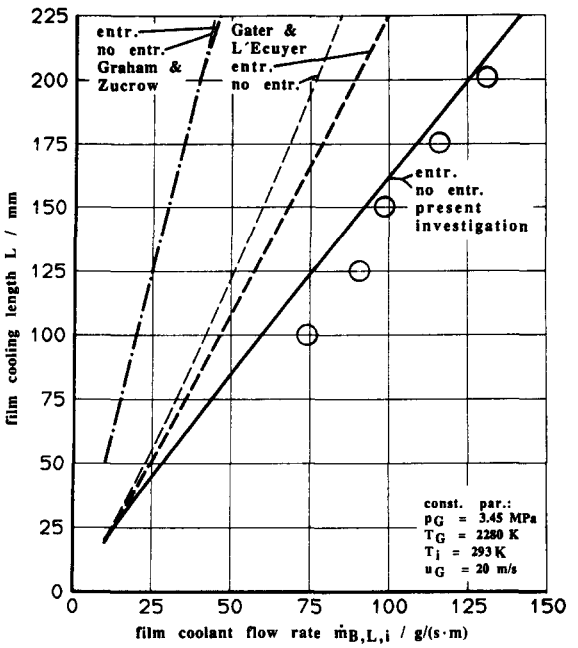

Figure 13. Comparison of previous experimental data and calculated values of several theoretical models.

values of interfacial shear stress than the present investigation. It can be seen that the agreement between the present model and the experimental data is satisfactory. The models of Graham & Zucrow (1957) and of Gater & L'Ecuyer (1969) produce film cooling lengths which are too long. The results for figure 12 concerning critical liquid mass flow rates and entrained fractions are the same here.

There is also a good agreement between the experimental data of Kinney & Sloop (1950), who worked at very high values of interfacial shear stress, and the theoretical results of the present investigation (Nahstoll 1988), which can not be demonstrated here in detail.

CONCLUSIONS

The new model for predicting the film cooling length has shown good agreement with the experimental results of the present investigation but also with previous experimental data. This model is superior to those known from the literature over a wide range of test conditions.

A detailed description of the interfacial phenomena produces better results without using results of special film cooling experiments for a global formulation of empirical correlations with only a narrow range of applicability.

REFERENCES

BURCK, E. 1969 Der Einfluß der Prandtlzahl auf den Wärmeübergang und Druckverlust künstlich aufgerauhter Strömungskanäle. *Wärme- u. Stoffübertrag.* **2,** 87–98.

CHAWLA, J. M. 1968 Reibungsdruckabfall bei der Strömung von Flüssigkeits-Gas-Gemischen in waagerechten Rohren. *Forsch. Geb. IngWes.* **34,** 47–54.

GATER, R. A. & L'ECUYER, M. R. 1969 A fundamental investigation of the phenomena that characterize liquid film cooling. Jet Propulsion Report TM-69-1, Purdue Univ., W. Lafayette, Ind.

GNIELINSKI, V. 1975 Neue Gleichungen für den Wärme- und Stoffübergang in turbulent durchströmten Rohren und Kanälen. *Forsch. Geb. IngWes.* **41,** 8–16.

GRAHAM, A. R. & ZUCROW, M. J. 1957 Film cooling, it's theory and application. Technical

Memorandum 57-3, Contract N7 OUR-39418, Jet Propulsion Center, Purdue Univ., W. Lafayette, Ind.

GREGORIG, R. 1970 Verallgemeinerter Ausdruck für den Einfluß temperaturabhängiger Stoffwerte auf den turbulenten Wärmeübergang. *Wärme- u. Stoffübertrag.* **3,** 26–40.

HOTTEL, H. C. SERAFIM, A. F. 1967 *Radiative Heat Transfer.* McGraw-Hill, New York.

HUGHMARK, G. A. 1973 Film thickness, entrainment and pressure drop in upward and dispersed flow. *AIChE Jl* **19,** 1062–1065.

KAYS, W. M. 1966 *Convective Heat and Mass Transfer.* McGraw-Hill, New York.

KAYS, W. M. 1972 Heat transfer to the transpired turbulent boundary layer. *Int. J. Heat Mass Transfer* **15,** 1023–1044.

KINNEY, G. R. & SLOOP, J. L. 1950 Internal film cooling experiments in a 4-inch duct with gas temperatures to 2000°F. NACA Report No. RM E52B19.

KRIEGEL, E. 1967 Berechnung von Zweiphasenströmungen von Gas/Flüssigkeitssystemen in Rohren. *Chemie-Ingr-Tech.* **39,** 1267–1274.

NAHSTOLL, J. 1988 Untersuchungen von Flüssigkeits-Filmströmungen bei hohen Verdampfungsraten im Hinblick auf Filmkühlung. Dissertation, Univ. of Kaiserslautern, F.R.G.

SHEARER C. J. & Nedderman, R. M. 1965 Pressure gradient and liquid film thickness in co-current upwards flow of gas/liquid mixtures: application to film cooler design. *Chem. Engng Sci.* **20,** 671–683.

VDI-WÄRMEATLAS 1984 VDI-Verlag, Düsseldorf, F.R.G.

WARNER, C. F. & EMMONS, D. L. 1964 Effect of selected gas stream parameters and coolant properties on liquid film cooling. *J. Heat Transfer* **86,** 271–278.

WHALLEY, P. B. & HEWITT, G. F. 1978 The correlation of liquid entrainment fraction and entrainment rate in annular two phase flow. Report AERE-R 9187, Harwell, U.K.

WOLFMÜLLER, K. 1984 Nichtlineare Regelung eines H_2/O_2 Dampfreaktors. Dissertation, Univ. of Karlsruhe, F.R.G.

WURZ, D. 1979 Wave velocity and wave structure at the surface of shear driven liquid rivulets. Presented at the *XIVth Biennial Fluid Dynamic Symp.*, Blazejewko, Poland.